

Tunneling spectroscopy of few-monolayer NbSe₂ in high magnetic field: Ising protection and triplet superconductivity

M. Kuzmanović,^{1,2,*} T. Dvir,^{3,*} D. LeBoeuf,⁴ S. Ilić,^{5,6}
 D. Möckli,^{3,7} M. Haim,³ S. Kraemer,⁴ M. Khodas,³ M. Houzet,⁵
 J. S. Meyer,⁵ M. Aprili,⁸ H. Steinberg,³ and C. H. L. Quay⁸

¹*Laboratoire de Physique des Solides (CNRS UMR 8502),
 Bâtiment 510, Université Paris-Saclay, 91405 Orsay, France*

²*QTF Centre of Excellence, Department of Applied Physics,
 Aalto University School of Science,
 P.O. Box 15100, 00076 Aalto, Finland*

³*Racah Institute of Physics, Hebrew University of Jerusalem,
 Givat Ram, Jerusalem 91904 Israel*

⁴*Laboratoire National des Champs Magnétiques Intenses (LNCMI-EMFL),
 CNRS, UGA, UPS, INSA, Grenoble/Toulouse, France*

⁵*Université Grenoble Alpes, CEA, Grenoble INP,
 IRIG, PHELIQS, 38000 Grenoble, France*

⁶*Centro de Física de Materiales (CFM-MPC),
 Centro Mixto CSIC-UPV/EHU, 20018 Donostia-San Sebastián, Spain*

⁷*Instituto de Física, Universidade Federal do Rio Grande do Sul,
 91501-970 Porto Alegre, RS, Brazil*

⁸*Laboratoire de Physique des Solides (CNRS UMR 8502),
 Bâtiment 510, Université Paris-Saclay, 91405 Orsay, France*

Abstract

Using van der Waals tunnel junctions, we perform spectroscopy of superconducting NbSe₂ flakes, of thicknesses ranging from 2–25 monolayers, measuring the quasiparticle density of states as a function of applied in-plane magnetic field up to 33T. In flakes up to ≈ 15 monolayers thick, we find that the density of states is well-described by a single band superconductor. In these thin samples, the magnetic field acts primarily on the spin (vs orbital) degree of freedom of the electrons, and superconductivity is further protected by Ising spin-orbit coupling (ISOC), which pins Cooper pair spins out-of-plane. The superconducting energy gap, extracted from our tunnelling spectra, decreases as a function of the applied magnetic field. However, in bilayer NbSe₂, close to the critical field (up to 30T, much larger than the Pauli limit), superconductivity appears to be even more robust than expected if only ISOC is considered. This can be explained by a predicted subdominant triplet component of the order parameter, coupled to the dominant singlet component at finite field. This equal-spin, odd-parity triplet state arises from the non-colinearity between the applied magnetic field and the Ising field.

PACS numbers:

I. INTRODUCTION

When bulk superconductors are subjected to an external applied magnetic field, the field is screened by circulating supercurrents, in what is known as the Meissner effect. The transition from the superconducting to the normal state occurs when the diamagnetic energy of the pairs exceeds the condensation energy. In 2D superconductors in parallel magnetic field, the Meissner effect is absent. Here the field acts only on the spin degree of freedom of electrons. In conventional (Bardeen-Cooper-Schrieffer or BCS) superconductors, due to the singlet wavefunction, the critical field H_c is set by the Pauli or Clogston-Chandrasekhar limit $\mu_B H_P = \Delta_0/\sqrt{2}$, where μ_B is the Bohr magneton and Δ_0 is the superconducting order parameter at zero field¹. The material becomes normal when the paramagnetic state of spin-aligned quasiparticles becomes more energetically favourable than the superconducting ground state².

Recently, superconductors of (few-)monolayer thicknesses have been obtained by exfoliation³ or single-layer deposition^{4,5}. Both show critical fields much larger than H_P ^{6,7}. In monolayer transition metal dicalcogenides such as 2H-NbSe₂ (hereafter NbSe₂) or gated 2H-MoS₂, this enhancement of the critical field is due in large part to spin-orbit coupling arising from the lack of in-plane crystal inversion symmetry^{8,9}. This gives rise to an out-of-plane Zeeman-equivalent magnetic field H_{SO} with opposite signs at the K and K' points of the hexagonal Brillouin zone¹⁰. In NbSe₂, $\mu_B H_{SO} = E_{SO} \approx 50$ meV for a monolayer. As it is invariant with respect to time-reversal (flipping both spin and momentum), this Zeeman valley-dependent field does not affect singlet superconductivity. It does however pin Cooper pair spins out-of-plane, hence the moniker ‘Ising (spin-orbit) field’^{11,12}. In the absence of a magnetic field, the superconducting wave-function is expected to show a mixture of odd-parity spin-singlet and even-parity spin-triplet components, with spin parts of the wavefunction respectively $\Phi_s = |\uparrow\downarrow\rangle - |\downarrow\uparrow\rangle$ and $\Phi_t = |\uparrow\downarrow\rangle + |\downarrow\uparrow\rangle$ ¹³. For E_{SO} smaller than the Fermi energy (E_F), the Φ_t triplet and Φ_s singlet decouple. The odd-parity triplet component Φ_t is thought not to coexist with the singlet component Φ_s ^{14,15}. (Even if Φ_t were energetically favourable, it would still be sensitive to disorder, and is suppressed when the mean free path is shorter than the superconducting coherence length¹⁶.)

An applied in-plane magnetic field H never completely aligns the Cooper pair spins in the plane even when the corresponding Zeeman energy $E_Z = \mu_B H \gg E_{SO}$. (Here, μ_B is

the Bohr magneton.) Thus, the in-plane critical field becomes much larger than $H_P^{6,11,12}$. Indeed, it diverges logarithmically at zero temperature^{8,17}. Because E_{SO} is larger than the inter-layer coupling, out-of-plane spin-locking persists in bilayer and few-monolayer TMDs¹⁸: the critical in-plane field H_c increases monotonically with diminishing NbSe₂ thickness down to the monolayer^{6,19}. Ising protection thus seems to be a quite general feature of NbSe₂ as intuited in early critical field studies²⁰.

Very recently, the pronounced two-fold anisotropy of the critical field, non-linear transport, and magneto-resistance of few- and mono-layer NbSe₂ devices close to the transition to the normal state have been interpreted as resulting from unconventional superconductivity^{21,22}: triplet components induced by the applied magnetic field and lateral lattice strain reduce the six-fold rotational symmetry expected from the hexagonal lattice to two-fold symmetry. Such triplets are essentially distinct from Φ_t considered above. They are induced by vector fields, and therefore come in pairs of partners transforming non-trivially under in-plane hexagonal symmetry. Previously, one such non-trivially transforming triplet of the form, $\Phi_{tB} = |\downarrow\downarrow\rangle + |\uparrow\uparrow\rangle$ ^{16,23,24} had been predicted to substantially affect the critical field²⁵. We report here tunnelling spectroscopy of few-layer NbSe₂ devices in a broad range of applied in-plane magnetic fields. As the magnetic field increases, our measurements progressively deviate from the prediction based on pure singlet pairing. We attribute this field-induced deviation to the onset of equal-spin triplet pairing in the form of Φ_{tB} .

II. RESULTS

Φ_{tB} arises from the non-collinearity of the spin-orbit field H_{SO} and the applied field H . This unpolarised equal-spin triplet component is coupled to linearly to the singlet Φ_s by the applied magnetic field, which means that with increasing fields Φ_s and Φ_{tB} strongly affect each other. Φ_{tB} is thus expressed, even when $\Delta_{tB} < \Delta_s$, and it is also robust to disorder. In contrast, Φ_t is decoupled from Φ_s at all fields and is not expressed for energetical reasons. Our model thus includes Φ_s and Φ_{tB} order parameters and neglects Φ_t . In the case where a finite pairing interaction is present in the Φ_{tB} channel as suggested by recent DFT calculations²⁶, assuming a single-band superconductor and neglecting inter-valley scattering, the superconducting energy gap Δ can be obtained from the quasiclassical theory of superconductivity (cf. Equation S9 in S.I.) :

$$\Delta = (E_{SO}\Delta_s + E_Z\Delta_{tB})/\sqrt{E_{SO}^2 + E_Z^2}, \quad (1)$$

where Δ_s and Δ_{tB} are, respectively, the singlet and equal-spin triplet order parameters. Here we can see that, compared to the case of Φ_s with Ising protection alone, the coexistence of Δ_{tB} with Δ_s and the coupling between the two can make superconductivity even more robust to an applied magnetic field. In the case where there is no pairing in the equal-spin triplet channel ($\Delta_{tB} = 0$), Δ is reduced by the applied magnetic field through the factor $E_{SO}/\sqrt{E_{SO}^2 + E_Z^2}$ and vanishes asymptotically, giving the afore-mentioned logarithmic divergence of the critical field at zero temperature. To obtain the order parameters Δ_s and Δ_{tB} at finite temperature and magnetic field, one has to solve two coupled equations self-consistently (cf. Supp. Info.). As we will show below, the inclusion of the field-induced equal-spin component Φ_{tB} boosts the critical magnetic field and provides a more accurate description of our spectroscopic data.

The quasiclassical theory also gives the density of states (DOS), which is found for $E < E_{SO}$ to be simply the BCS DOS, with the gap as in Equation 1 (see Equation 14 in the Supp. Info.). Note that, unlike 2D superconductors with low spin-orbit coupling in in-plane fields, the coherence peak is not Zeeman-split²⁷. In addition, the Ising protection results in a sharp BCS coherence peak in the DOS, regardless of the strength of the triplet coupling or the applied magnetic field. Nevertheless, in the presence of inter-valley scattering (τ being the inter-valley scattering time), the density of states is smeared out¹⁵ as in the Abrikosov-Gor'kov theory^{28,29}. Thus inter-valley scattering not only reduces Ising protection by averaging over valleys with opposite signs of E_{SO} , it also modifies the shape of the DOS and regularizes the divergence of the critical field at zero temperature¹⁷. Finally, in the limit of strong inter-valley scattering ($1/\tau \gg \Delta_s$) that doesn't correspond to our experimental situation (in which $1/\tau \sim \Delta_s$), the dependence of Δ on the applied magnetic field becomes similar to that expected from the Abrikosov-Gor'kov theory with the critical field given by $\mu_B H_c = E_{SO}\sqrt{2\Delta\tau/\hbar}$.

We fabricate tunnel junctions (J1 to J7) on superconducting NbSe₂ flakes of 1.2–50 nm thickness. The tunnel barriers are thin flakes of semiconducting WSe₂ or MoS₂ exfoliated by the van der Waals dry transfer technique described in Ref.³⁰. A Ti/Au normal counter electrode is then evaporated on the semiconductor leading to a structure shown schematically in Figure 1(a). An ohmic contact to the NbSe₂ is also fabricated. The typical surface area

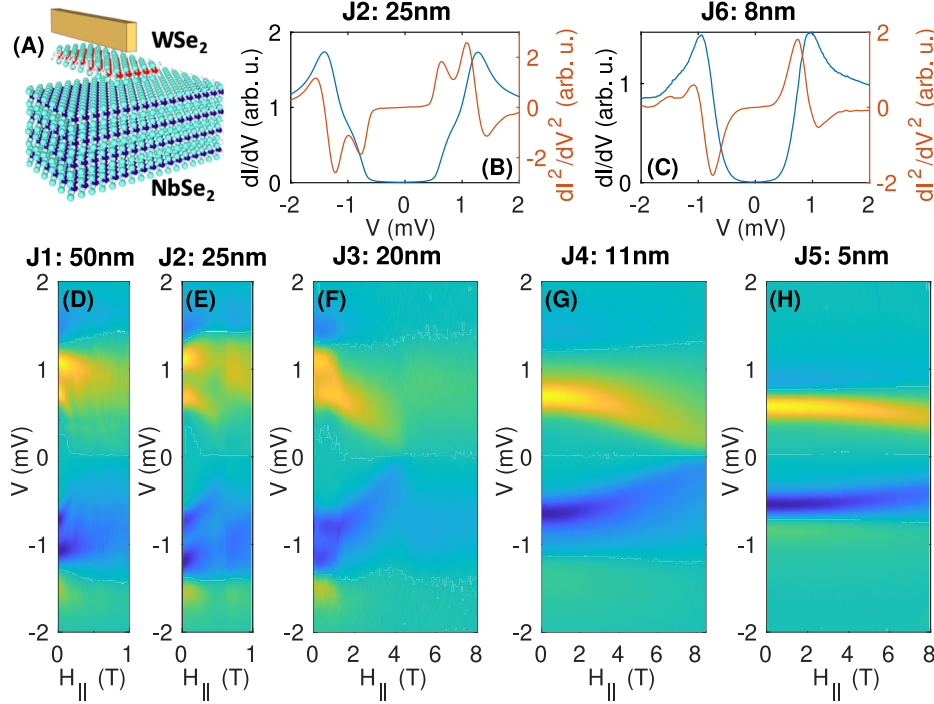


FIG. 1: Tunneling spectroscopy of bulk and few-monolayer NbSe₂ through van der Waals barriers. (a) Schematic drawing of the tunnel junction: few layer- NbSe₂, covered with thin WSe₂ (or MoS₂) and a Ti/Au electrode. (b) Differential conductance ($G = dI/dV$) as a function of bias voltage (V) of J2 (blue) and d^2I/dV^2 vs V of J2 (red). (c) Same as panel (b) for J6. (d)-(h) Colormaps of the magnetic field dependence of the d^2I/dV^2 curves for Junctions 1-5. All measurements were taken at temperatures of 30-70 mK.

of the junction is about $1 \mu\text{m}^2$ and the resistance in the normal state $>10 \text{ k}\Omega$. The critical temperature T_c decreases from 7.2 K in the thickest flakes to $\sim 2.6 \text{ K}$ in the thinnest ones.

Using standard lock-in techniques, we first measure the current I and differential conductance $G = dI/dV$ across the junctions as a function of applied bias voltage V ³¹ and in-plane magnetic fields H in dilution refrigerators with base temperatures of 30–70 mK. $G(V)$ is proportional to the DOS convolved with the derivative of the Fermi distribution function³². Therefore, in principle, the energy resolution of our spectroscopy is given by the temperature and the integrated voltage noise across the junction.

Typical $G(V)$ curves are shown for a 25 nm thick sample (J2) and a 6 monolayer sample (J6) in Figure 1(b,c), top panels. The main differences between these junctions are: (1) the smaller superconducting gap in the thinner device due to a smaller T_c , and (2) the low-energy

shoulder, very clearly seen in the thicker junction, is absent in the thinner one. This is even more apparent in the second derivative of the current as a function of the voltage bias, dG/dV , in figure 1(b,c): the two peaks in J2, merge to a single peak in J6. This merging was previously observed^{30,33} and it is now shown to persist in flakes up to 11 nm (≈ 15 monolayer) thick: the two-band superconductivity of bulk NbSe₂³⁴ is lost. A single-band theory thus seems most suitable for the thinnest flakes.

Figures 1(d-h) show the evolution of the dG/dV curves of five junctions (J1-J5) with increasing in-plane magnetic field. Junctions 1 and 2, the thickest, show similar responses to the applied field: the inner peak shifts to lower energies faster than the outer peak. This is consistent with previous experiments, and is likely due to the 3D character of the Se p_z -orbital-derived band at the Γ point, which is associated with the smaller superconducting energy gap, as well as its higher diffusion coefficient^{30,35}. For the thinner junctions, J4 and J5, a single gap persists from zero field up to 9 T in agreement with recent results on MoS₂³⁶. As noted above, the robustness of the gap to applied magnetic fields is expected in thin samples due to Ising protection and drastically reduced orbital depairing. To significantly reduce the gap and to study the effect of the applied field on the density of states it is necessary to go to even higher fields.

Therefore, we measure two tunnel junctions (J6, 6-monolayer) and (J7, bilayer) in in-plane magnetic fields of up to 33 T at 1.3 K (pumped liquid helium). Their critical temperatures are, respectively, 5.4 K ($H_P = 10.5T$) and 2.6 K ($H_P = 5T$), giving $\Delta/k_B T_c \approx 1.8$, close to the BCS prediction and in agreement with previous studies³⁰. Finally, the critical in-plane fields are $H_c = 18$ T for J6 and $H_c = 30$ T for J7, corresponding respectively to $H_c = 1.5H_P$ and $H_c = 6H_P$. (See Figure 3.) These junctions had earlier been characterized at 50mK (dilution refrigerator) at zero magnetic field (Figures 2(a) and (d)) — hard gaps were observed, pointing to tunneling as the main transport mechanism. These tunnel spectra are well-described by a fit to a BCS density of states, broadened by a $\sim 200\mu eV$ effective temperature. (The fact that this is much larger than 50mK is addressed below.)

III. DISCUSSION

The evolution of $G(V)$ with the in-plane magnetic field at 1.3K is shown in Figures 2(a) (J6) and 2(d) (J7). For clarity, spectra at selected magnetic fields are also shown in

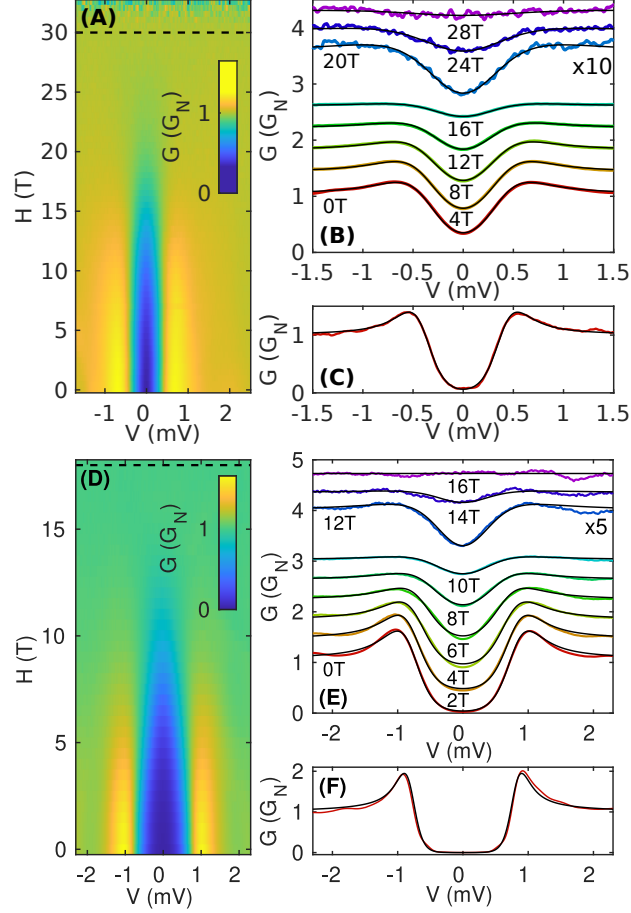


FIG. 2: Differential conductance $G = dI/dV$ as a function of the voltage V and of the in-plane magnetic field H of J6 (6 monolayers) and J7 (bilayer). The tunneling spectra are normalized by the normal state conductance, $G_N(V)$, measured above H_c . (a,d) Colormap of $G(V)$ as a function of field at $T = 1.3$ K. The dotted lines indicate the critical fields. (b,e) Horizontal slices of the data in the colormaps (a) and (d) respectively, showing $G(V)$ at different fields, vertically displaced for clarity. The black lines are fits to an Abrikosov-Gor'kov-like density of states, with the energy gap and A-G broadening parameter as fitting parameters. (c,f) Data at $T = 50$ mK and zero magnetic field (red lines) together with the fits obtained using a BCS DOS and an effective temperature (black links). The superconducting gaps obtained from the fits are, respectively, $400\mu\text{eV}$ and $800\mu\text{eV}$, while the temperatures are respectively 1K and 0.9K.

Figures 2(b) and 2(e) together with an Abrikosov-Gor'kov-like density of states with a field-dependent broadening parameter^{29,37}, convolved with a Fermi function to account for the temperature. The fits account remarkably well for the experimental data.

The superconducting gaps obtained from these fits are shown as a function of the in-plane magnetic field in Figure 3. (Note that in the case of bilayer NbSe₂ close to H_c , the Zeeman and ISOC energy scales are much larger than Δ_0 .) In the same figure we also plot the theoretical curves calculated at $T = 1.3$ K using the Ising model with and without a triplet subdominant component of the order parameter as described above (i.e. $\Delta_{tB} \neq 0$ and $\Delta_{tB} = 0$ respectively). The fitting parameters are given in the caption of Figure 3. Note that, for the bilayer device (J7), the temperature of the experiment (1.3K) is higher than the critical temperature of the triplet component ($T_{ct} = 0.05T_{cs} = 130mK$, obtained from the fit). Therefore, the triplet order parameter Δ_{tB} exists only through its coupling with the singlet order parameter Δ_s .

Focusing on the thinner, bilayer device (J7), we see that the Ising theory alone (without triplet) fits the data reasonably well up to about 20T, but not close to the critical field, where the superconducting energy gap is more robust than expected. This is very suggestive of a second order parameter revealed as the dominant order parameter disappears¹⁴. Indeed introducing a small triplet component of the gap, a better fit of the overall experimental data is obtained. As the experiment is carried out above the triplet critical temperature, the main effect of triplet pairing is to enhance the critical field through the coupling with the singlet order parameter. In addition, the triplet subdominant component also renders the gap vs. field dependence more linear. This is in contrast to what is expected in an Ising theory including strong inter-valley scattering (equivalent to Abrikosov-Gor'kov), which is also shown for completeness in Figure 3, where the only fitting parameter is the critical field. For the thicker device (J6) a triplet component does not significantly change the fit. This is perhaps due to a smaller E_{SO} and a smaller critical field.

Finally, we address the issue of in-gap states and the broadening of the coherence peaks. Indeed, the broadening parameters obtained from the fits are larger than expected from self-consistent Abrikosov-Gor'kov theory (see Supp. Info.), and at the critical field the broadening parameter is larger than theoretically allowed. There are several possible reasons for DOS broadening: (1) A slight misalignment of the applied magnetic field (leading to pair-breaking). A misalignment of $\sim 1^\circ$ (the maximum possible in our experiment), gives a perpendicular component of the magnetic field smaller than 0.3 T, several times smaller than the perpendicular critical field³⁸. (2) Nodes in the gap. In-gap states may appear in triplet superconductors because of field-induced gap nodes at the Fermi surface³⁹. If they

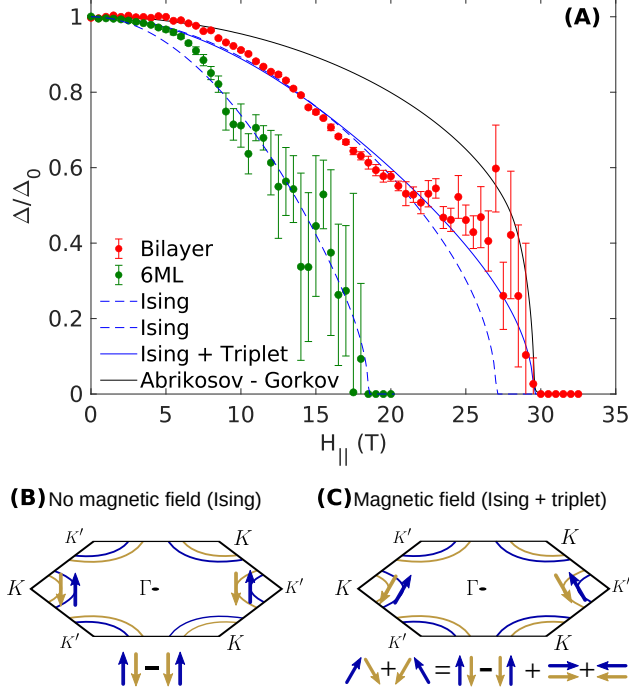


FIG. 3: Equal-spin triplet superconductivity (a) Normalized superconducting energy gap as a function of the in-plane magnetic field obtained from the fits of the quasiparticle density of states in Figure 2. The error bars have been calculated following the procedure described in the Supp. Info. The blue lines are a fit of experimental data using the Ising theory with (solid) and without (dashed) an equal-spin triplet component of the order parameter as described in the text. For the bilayer, in the Ising fit, $E_{SO} = 14.45T_{cs}$; in Ising with triplet fit $E_{SO} = 9.62T_{cs}$ and $T_{ct} = 0.05T_{cs}$, where $T_{cs} = 2.6K$. For the 6-monolayer, $E_{SO} = 2.21T_{cs}$, where $T_{cs} = 5.4K$. The solid black line is the calculated $\Delta(H)$ curve using the Ising theory with strong disorder (equivalent to the Abrikosov-Gor'kov theory), setting the critical field to the experimental one. (b) At zero magnetic field, singlet Cooper pairs form from electrons at opposite corners of the Brouillon zone (K and K' points). Their spins are pinned out-of-plane by the Ising field. (c) An in-plane magnetic field partially aligns electron spins orthogonal to the Ising field, and gives rise to equal-spin triplet pairs.

exist, such nodes are expected along the Γ -M direction and are thus related to multiband effects. (3) Inelastic tunneling. (4) Coupling of the charge density waves via phonons either to the quasiparticles, or to amplitude fluctuations (Higgs mode) of the order parameters⁴⁰. These various factors are difficult to disentangle; however, none of them significantly affects the energy gap, which can be determined with high precision from the fits. (See Supp. Info.

for more details.)

While previous reports on Andreev spectroscopy experiments have shown a reduction of the gap consistent with field-induced depairing in the presence of Ising protection⁴¹, our hard-gap tunnel junctions allow a quantitative analysis of the main microscopic mechanism for the enhancement of the critical field, pointing to possible equal-spin triplet superconductivity. Within the scenarios of Refs.^{21,22} the triplet order parameters allowed by symmetry such as Φ_{tB} are nearly degenerate with the leading singlet order parameter. Attraction in the triplet channel is supported by recent DFT calculations²⁶; however, there is at present no evidence of near degeneracy between triplet and singlet channels. Our interpretation does not require near degeneracy, and the singlet-triplet coupling comes from a clear microscopic mechanism (the in-plane magnetic field), which is quantitatively accounted for both in the theory and in the analysis of the experimental data.

Further study at even lower temperatures and of a new generation of devices with different barrier materials will be required to unambiguously confirm the existence of equal-spin triplets in $NbSe_2$.

IV. MATERIALS AND METHODS

Especially at high magnetic fields, special care was taken to ensure that the applied magnetic field is parallel to the flakes. It is aligned to better than $\sim 1^\circ$. In addition, we checked that the voltage noise due to mechanical vibrations is lower than that from the thermal broadening. This is described in detail in the Supp. Info.

V. ACKNOWLEDGEMENTS

We acknowledge valuable discussions with Pascal Simon and Freek Massee, and thank the latter for a careful reading of the manuscript. This work was funded by a Maimonides-Israel grant from the Israeli-French High Council for Scientific and Technological Research, ANR JCJC (SPINOES) and ANR PIRE (HYBRID) grants from the French Agence Nationale de Recherche, ERC Starting Grant ERC-2014-STG 637928 (TUNNEL), Israel Science Foundation Grants No.s 861/19 and 2665/20, and the Laboratoire d'Excellence LANEF in Grenoble (ANR10-LABX-51-01). T.D. is grateful to the Azrieli Foundation for an Azrieli Fellowship.

Part of this work has been performed at the Laboratoire National de Champs Magnétiques Intenses (LNCMI), a member of the European Magnetic Field Laboratory (EMFL).

* These two authors contributed equally

- ¹ Clogston, A. M. Upper Limit for the Critical Field in Hard Superconductors. Physical Review Letters **9**, 266–267 (1962). URL <https://link.aps.org/doi/10.1103/PhysRevLett.9.266>. Publisher: American Physical Society.
- ² Fulde, P. High field superconductivity in thin films. Advances in Physics **22**, 667–719 (1973). URL <http://www.tandfonline.com/doi/abs/10.1080/00018737300101369>.
- ³ Wang, Q. H., Kalantar-Zadeh, K., Kis, A., Coleman, J. N. & Strano, M. S. Electronics and optoelectronics of two-dimensional transition metal dichalcogenides. Nature Nanotechnology **7**, 699–712 (2012). URL <https://www.nature.com/articles/nnano.2012.193>. Number: 11 Publisher: Nature Publishing Group.
- ⁴ Zhang, T. et al. Superconductivity in one-atomic-layer metal films grown on Si(111). Nature Physics **6**, 104–108 (2010). URL <https://www.nature.com/articles/nphys1499>. Number: 2 Publisher: Nature Publishing Group.
- ⁵ Fan, Q. et al. Plain s-wave superconductivity in single-layer FeSe on SrTiO₃ probed by scanning tunnelling microscopy. Nature Physics **11**, 946–952 (2015). URL <https://www.nature.com/articles/nphys3450>. Number: 11 Publisher: Nature Publishing Group.
- ⁶ Xi, X. et al. Ising pairing in superconducting NbSe₂ atomic layers. Nature Physics **12**, 139–143 (2016). URL <https://www.nature.com/articles/nphys3538>. Number: 2 Publisher: Nature Publishing Group.
- ⁷ Liu, Y. et al. Interface-Induced Zeeman-Protected Superconductivity in Ultrathin Crystalline Lead Films. Physical Review X **8**, 021002 (2018). URL <https://link.aps.org/doi/10.1103/PhysRevX.8.021002>. Publisher: American Physical Society.
- ⁸ Frigeri, P. A., Agterberg, D. F. & Sigrist, M. Spin susceptibility in superconductors without inversion symmetry. New Journal of Physics **6**, 115 (2004). URL <http://iopscience.iop.org/article/10.1088/1367-2630/6/1/115/meta>. Publisher: IOP Publishing.
- ⁹ Gor'kov, L. P. & Rashba, E. I. Superconducting 2D System with Lifted Spin Degeneracy: Mixed Singlet-Triplet State. Physical Review Letters **87**, 037004 (2001). URL <https://link.aps.org/doi/10.1103/PhysRevLett.87.037004>.

- aps.org/doi/10.1103/PhysRevLett.87.037004. Publisher: American Physical Society.
- ¹⁰ Xu, X., Yao, W., Xiao, D. & Heinz, T. F. Spin and pseudospins in layered transition metal dichalcogenides. Nature Physics **10**, 343–350 (2014). URL <https://www.nature.com/articles/nphys2942>. Number: 5 Publisher: Nature Publishing Group.
 - ¹¹ Saito, Y. et al. Superconductivity protected by spin–valley locking in ion-gated MoS₂. Nature Physics **12**, 144–149 (2016). URL <https://www.nature.com/articles/nphys3580>.
 - ¹² Lu, J. M. et al. Evidence for two-dimensional Ising superconductivity in gated MoS₂. Science **350**, 1353–1357 (2015). URL <https://science.sciencemag.org/content/350/6266/1353>.
 - ¹³ Smidman, M., Salamon, M. B., Yuan, H. Q. & Agterberg, D. F. Superconductivity and spin–orbit coupling in non-centrosymmetric materials: a review. Reports on Progress in Physics **80**, 036501 (2017). URL <https://doi.org/10.1088/1361-6633/80/3/036501>.
 - ¹⁴ Rainer, D., Burkhardt, H., Fogelström, M. & Sauls, J. A. Andreev bound states, surfaces and subdominant pairing in high T_c superconductors. Journal of Physics and Chemistry of Solids **59**, 2040–2044 (1998). URL <https://www.sciencedirect.com/science/article/pii/S0022369798001759>.
 - ¹⁵ Haim, M., Möckli, D. & Khodas, M. Signatures of triplet correlations in density of states of ising superconductors. Phys. Rev. B **102**, 214513 (2020). URL <https://link.aps.org/doi/10.1103/PhysRevB.102.214513>.
 - ¹⁶ Möckli, D. & Khodas, M. Ising superconductors: Interplay of magnetic field, triplet channels, and disorder. Physical Review B **101**, 014510 (2020). URL <https://link.aps.org/doi/10.1103/PhysRevB.101.014510>.
 - ¹⁷ Ilić, S., Meyer, J. S. & Houzet, M. Enhancement of the Upper Critical Field in Disordered Transition Metal Dichalcogenide Monolayers. Physical Review Letters **119**, 117001 (2017). URL <https://link.aps.org/doi/10.1103/PhysRevLett.119.117001>. Publisher: American Physical Society.
 - ¹⁸ Jones, A. M. et al. Spin–layer locking effects in optical orientation of exciton spin in bilayer WSe₂. Nature Physics **10**, 130–134 (2014). URL <https://www.nature.com/articles/nphys2848>. Number: 2 Publisher: Nature Publishing Group.
 - ¹⁹ de la Barrera, S. C. et al. Tuning Ising superconductivity with layer and spin–orbit coupling in two-dimensional transition-metal dichalcogenides. Nature Communications **9**, 1427 (2018). URL <https://www.nature.com/articles/s41467-018-03888-4>. Number: 1 Publisher: Na-

ture Publishing Group.

- ²⁰ Prober, D. E., Schwall, R. E. & Beasley, M. R. Upper critical fields and reduced dimensionality of the superconducting layered compounds. Physical Review B **21**, 2717–2733 (1980). URL <https://link.aps.org/doi/10.1103/PhysRevB.21.2717>. Publisher: American Physical Society.
- ²¹ Hamill, A. et al. Unexpected two-fold symmetric superconductivity in few-layer nbse₂. arXiv:2004.02999 (2020). URL <https://arxiv.org/abs/2004.02999>. ArXiv: 2004.02999.
- ²² Cho, C.-W. et al. Distinct nodal and nematic superconducting phases in the 2D Ising superconductor NbSe₂. arxiv:2003.12467 (2020).
- ²³ Tang, G., Bruder, C. & Belzig, W. Magnetic field-induced "mirage" gap in an Ising superconductor. arXiv:2011.07080 [cond-mat] (2020). URL <http://arxiv.org/abs/2011.07080>. ArXiv: 2011.07080.
- ²⁴ Nakamura, Y. & Yanase, Y. Odd-parity superconductivity in bilayer transition metal dichalcogenides. Physical Review B **96**, 054501 (2017). URL <https://link.aps.org/doi/10.1103/PhysRevB.96.054501>. Publisher: American Physical Society.
- ²⁵ Möckli, D. & Khodas, M. Magnetic-field induced $s+\mathit{if}$ pairing in Ising superconductors. Physical Review B **99**, 180505 (2019). URL <https://link.aps.org/doi/10.1103/PhysRevB.99.180505>.
- ²⁶ Wickramaratne, D., Khmelevskyi, S., Agterberg, D. F. & Mazin, I. Ising Superconductivity and Magnetism in NbSe_2 . Physical Review X **10**, 041003 (2020). URL <https://link.aps.org/doi/10.1103/PhysRevX.10.041003>.
- ²⁷ Meservey, R., Tedrow, P. M. & Fulde, P. Magnetic Field Splitting of the Quasiparticle States in Superconducting Aluminum Films. Physical Review Letters **25**, 1270–1272 (1970). URL <http://link.aps.org/doi/10.1103/PhysRevLett.25.1270>.
- ²⁸ Bruno, R. C. & Schwartz, B. B. Magnetic Field Splitting of the Density of States of Thin Superconductors. Physical Review B **8**, 3161–3178 (1973). URL <https://link.aps.org/doi/10.1103/PhysRevB.8.3161>.
- ²⁹ Abrikosov, A. A. & Gor'kov, L. P. Contribution to the theory of superconducting alloys with paramagnetic impurities. JETP **12**, 1243 (1961).
- ³⁰ Dvir, T. et al. Spectroscopy of bulk and few-layer superconducting NbSe₂ with van der Waals tunnel junctions. Nature Communications **9**, 598 (2018). URL <https://www.nature.com/articles/s41467-018-03000-w>. Number: 1 Publisher: Nature Publishing Group.

- ³¹ Giaever, I. Energy Gap in Superconductors Measured by Electron Tunneling. Physical Review Letters **5**, 147–148 (1960). URL <https://link.aps.org/doi/10.1103/PhysRevLett.5.147>. Publisher: American Physical Society.
- ³² Tinkham, M. Introduction to Superconductivity (Dover, Mineola, 1996), 2 edn.
- ³³ Khestanova, E. et al. Unusual Suppression of the Superconducting Energy Gap and Critical Temperature in Atomically Thin NbSe₂. Nano Letters **18**, 2623–2629 (2018). URL <https://doi.org/10.1021/acs.nanolett.8b00443>. Publisher: American Chemical Society.
- ³⁴ Noat, Y. et al. Quasiparticle spectra of $2H-\mathrm{NbSe}_2$: Two-band superconductivity and the role of tunneling selectivity. Physical Review B **92**, 134510 (2015). URL <https://link.aps.org/doi/10.1103/PhysRevB.92.134510>. Publisher: American Physical Society.
- ³⁵ Dvir, T., Aprili, M., Quay, C. H. L. & Steinberg, H. Tunneling into the Vortex State of NbSe₂ with van der Waals Junctions. Nano Letters **18**, 7845–7850 (2018). URL <https://doi.org/10.1021/acs.nanolett.8b03605>. Publisher: American Chemical Society.
- ³⁶ Costanzo, D., Zhang, H., Reddy, B. A., Berger, H. & Morpurgo, A. F. Tunnelling spectroscopy of gate-induced superconductivity in MoS₂. Nature Nanotechnology **13**, 483–488 (2018). URL <https://www.nature.com/articles/s41565-018-0122-2>. Number: 6 Publisher: Nature Publishing Group.
- ³⁷ Srivastava, R. V. A. & Teizer, W. Analytical density of states in the Abrikosov-Gorkov theory. Solid State Communications **145**, 512–513 (2008). URL <https://www.sciencedirect.com/science/article/pii/S0038109807008344>.
- ³⁸ Tsen, A. W. et al. Nature of the quantum metal in a two-dimensional crystalline superconductor. Nature Physics **12**, 208–212 (2016). URL <https://www.nature.com/articles/nphys3579>. Number: 3 Publisher: Nature Publishing Group.
- ³⁹ Fischer, M. H., Sigrist, M. & Agterberg, D. F. Superconductivity without Inversion and Time-Reversal Symmetries. Physical Review Letters **121**, 157003 (2018). URL <https://link.aps.org/doi/10.1103/PhysRevLett.121.157003>. Publisher: American Physical Society.
- ⁴⁰ Littlewood, P. B. & Varma, C. M. Amplitude collective modes in superconductors and their coupling to charge-density waves. Physical Review B **26**, 4883–4893 (1982). URL <https://link.aps.org/doi/10.1103/PhysRevB.26.4883>. Publisher: American Physical Society.
- ⁴¹ Sohn, E. et al. An unusual continuous paramagnetic-limited superconducting phase transition in

2D NbSe 2. Nature Materials **17**, 504–508 (2018). URL <https://www.nature.com/articles/s41563-018-0061-1>. Number: 6 Publisher: Nature Publishing Group.

SUPPLEMENTAL MATERIALS for

“Tunneling spectroscopy of few-monolayer NbSe₂ in high magnetic field: Ising protection and triplet superconductivity”

M. Kuzmanović,^{1,2,*} T. Dvir,^{3,*} D. LeBoeuf,⁴ S. Ilić,^{5,6} D. Möckli,^{3,7} M. Haim,³ S. Kraemer,⁴
M. Khodas,³ M. Houzet,⁵ J. S. Meyer,⁵ M. Aprili,⁸ H. Steinberg,³ and C. H. L. Quay⁸

¹*Laboratoire de Physique des Solides (CNRS UMR 8502),
Bâtiment 510, Université Paris-Saclay, 91405 Orsay, France*

²*QTF Centre of Excellence, Department of Applied Physics,
Aalto University School of Science, P.O. Box 15100, 00076 Aalto, Finland*

³*Racah Institute of Physics, Hebrew University of Jerusalem, Givat Ram, Jerusalem 91904 Israel*

⁴*Laboratoire National des Champs Magnétiques Intenses (LNCMI-EMFL),
CNRS, UGA, UPS, INSA, Grenoble/Toulouse, France*

⁵*Université Grenoble Alpes, CEA, Grenoble INP, IRIG, PHELIQS, 38000 Grenoble, France*

⁶*Centro de Física de Materiales (CFM-MPC), Centro Mixto CSIC-UPV/EHU, 20018 Donostia-San Sebastián, Spain*

⁷*Instituto de Física, Universidade Federal do Rio Grande do Sul, 91501-970 Porto Alegre, RS, Brazil*

⁸*Laboratoire de Physique des Solides (CNRS UMR 8502),
Bâtiment 510, Université Paris-Saclay, 91405 Orsay, France*

PACS numbers:

I. THEORY

In this appendix, we calculate the superconducting energy gap of a monolayer superconductor without an inversion center and in the presence of an in-plane magnetic Zeeman field. We first present the appropriate Hamiltonian. Then, we obtain the quasi-classical Green functions for the case where there is only intra-valley scattering. We derive expressions for the density of states and the coupled self-consistency equations for the singlet and triplet order parameter in the limit of large spin-orbit coupling^{S1}, which allow us to compute the energy gap as a function of magnetic field and fit the experimental data. The effect of inter-valley disorder is studied using a Landau expansion^{S2} to obtain the thermodynamic potential. Minimization of the thermodynamic potential yields the thermodynamic order parameters (OPs) which are used in the calculation of the energy gap.

A. The model Hamiltonian

Our model is defined by the Hamiltonian which describes the band structure, the effects of the spin-orbit interaction, the applied parallel magnetic field, the pairing interaction, and the disorder potential. A single energy band crosses the Fermi level, which gives rise to the three hole pockets in the absence of the spin-orbit interaction. One large hole pocket is centered at the Γ point, and the pair of pockets related via the time reversal symmetry are located at the K and K' valleys. Most of the thermodynamics properties of NbSe₂ monolayers can be reliably addressed within a simplified model retaining only the pockets centred at K and K' valleys. The magnitude of the spin-orbit splitting is constant in this case. Unlike in the bulk, in monolayers bands derived from the Se p orbitals do not cross the Fermi level. The transition metal ions such as Nb produce a noticeable atomic spin-orbit interaction. As a result, since the mono-layer lacks the inversion symmetry, the bands are spin-split except along the high symmetry ΓM -lines, where the horizontal and vertical mirror planes cross. The model Hamiltonian reads

$$\begin{aligned}
 H = & \sum_{\mathbf{k},s} \xi_{\mathbf{k}} c_{\mathbf{k}s}^\dagger c_{\mathbf{k}s} + \sum_{\mathbf{k},ss'} [\gamma(\mathbf{k}) - \mathbf{B}] \cdot \boldsymbol{\sigma}_{ss'} c_{\mathbf{k}s}^\dagger c_{\mathbf{k}s'} \\
 & + \frac{1}{2} \sum_{\mathbf{k},\mathbf{k}'} \sum_{\{s_i,s'_i\}} V_{s_1 s_2}^{s_1 s_2}(\mathbf{k},\mathbf{k}') c_{\mathbf{k}s_1}^\dagger c_{-\mathbf{k}s_2}^\dagger c_{-\mathbf{k}'s'_2} c_{\mathbf{k}'s'_1} \\
 & + \frac{1}{2} \sum_{\mathbf{k},\mathbf{k}'} \sum_s U_0(\mathbf{k} - \mathbf{k}') c_{\mathbf{k}s}^\dagger c_{\mathbf{k}'s},
 \end{aligned} \tag{S1}$$

where $c_{\mathbf{k}s}^\dagger = V^{-1/2} \int d\mathbf{r} e^{i\mathbf{k}\cdot\mathbf{r}} \psi_{\mathbf{r}s}^\dagger$ and the operator $\psi_{\mathbf{r}s}^\dagger$ creates a particle with spin projection s along the z -axis at position \mathbf{r} in a volume V . Here, $\xi(\mathbf{k}) = \xi(-\mathbf{k})$ is the dispersion measured from the chemical potential, $\gamma(-\mathbf{k}) = -\gamma(\mathbf{k})$

is the spin-orbit coupling (SOC) present in a lattice lacking an inversion center, and $\mathbf{B} = E_Z \hat{x}$ is the Zeeman field, where E_Z absorbs the prefactor $g\mu_B/2$ with the g -factor and the Bohr magneton, and has dimension of energy. The vector of Pauli matrices is denoted by $\boldsymbol{\sigma} = (\sigma_1, \sigma_2, \sigma_3)$. The superconducting pairing interaction $V_{s'_1 s'_2}^{s_1 s_2}(\mathbf{k}, \mathbf{k}')$ contains the pairing channels allowed by the lattice symmetry.

The presence of randomly distributed scalar impurities gives rise to a scattering potential $U_0(\mathbf{k} - \mathbf{k}')$. Singlet pairing as well as inter-valley triplet pairing is not sensitive to intra-valley scattering. To study the effect of inter-valley scattering, we consider a short-range impurity potential such that $U_0(\mathbf{k} - \mathbf{k}') = U_0$. The effect of the impurity potential is described within the self-consistent Born approximation by the appropriate self-energy $\hat{\Sigma}$, which we do not write here explicitly. $\hat{\Sigma}$ is proportional to the scattering rate $\Gamma = \pi n_{imp} N_0 U_0^2$, where n_{imp} is the impurity density and N_0 is the normal state density of states per spin species. In the following, we set $k_B = 1$.

The SOC has the form $\boldsymbol{\gamma}(\mathbf{k}) = E_{SO} \hat{\gamma}(\mathbf{k}) \hat{z}$. Here we consider the simplest model for nodeless SOC $\hat{\gamma}(\mathbf{k}) = \text{sgn}[\cos(3\varphi_{\mathbf{k}})]$, where $\varphi_{\mathbf{k}}$ is the angle the vector \mathbf{k} forms with the k_x axis. Along the Fermi surface centered at Γ the SOC $\hat{\gamma}(\mathbf{k})$ changes sign six times at the ΓM lines. The SOC is constant and antiparallel at the pockets centered at K and K' valleys. In order to reduce the Hamiltonian to be quadratic in the field operators, we perform a mean field decoupling of the pairing interaction part and define the self-consistent order parameter

$$\Delta_{s_1 s_2}(\mathbf{k}) = \frac{1}{V} \sum_{\mathbf{k}', s'_1, s'_2} V_{s'_1 s'_2}^{s_1 s_2}(\mathbf{k}, \mathbf{k}') \langle c_{-\mathbf{k}', s'_2} c_{\mathbf{k}', s'_1} \rangle. \quad (\text{S2})$$

We organize the superconducting OPs in the standard matrix form as

$$\Delta(\mathbf{k}) = [\psi(\mathbf{k}) + \mathbf{d}(\mathbf{k}) \cdot \boldsymbol{\sigma}] i\sigma_2. \quad (\text{S3})$$

Here $\psi(\mathbf{k})$ and $\mathbf{d}(\mathbf{k})$ parametrize the singlet and triplet components of the OP respectively. We neglect singlet anisotropy, setting $\psi(\mathbf{k}) = \Delta_s$. The symmetry of the system characterizes the triplet OP component as

$$\mathbf{d}(\mathbf{k}) = \hat{\gamma}(\mathbf{k}) (\eta_{E1} \hat{x} + \eta_{E2} \hat{y} + \eta_A \hat{z}) \quad (\text{S4})$$

and leads us to the effective interaction

$$\begin{aligned} V_{s'_1 s'_2}^{s_1 s_2}(\mathbf{k}, \mathbf{k}') &= v_s [i\sigma_2]_{s_1 s_2} [i\sigma_2]_{s'_1 s'_2}^* \\ &+ \sum_{j=1,2} v_t [\hat{\gamma}(\mathbf{k}) \sigma_j i\sigma_2]_{s_1 s_2} [\hat{\gamma}(\mathbf{k}') \sigma_j i\sigma_2]_{s'_1 s'_2}^* \\ &+ v_{tz} [\hat{\gamma}(\mathbf{k}) \sigma_3 i\sigma_2]_{s_1 s_2} [\hat{\gamma}(\mathbf{k}') \sigma_3 i\sigma_2]_{s'_1 s'_2}^*. \end{aligned} \quad (\text{S5})$$

As shown in Ref.^{S3} the magnetic field couples the singlet order parameter Δ_s and the equal spin triplet order parameter η_{E2} . For the purpose of fitting the data, we assume that singlet pairing is dominant and that the temperatures is larger than the critical temperature of all the possible triplet pairings. In that case, we can set $\eta_A = \eta_{E1} = 0$ and keep only the singlet and the η_{E2} -triplet order parameters.

We define the transition temperature T_{cs} (T_{ct}) by setting $E_Z = E_{SO} = \Gamma = 0$ and keeping only the $\Delta_s(\eta_{E2})$ OP in Eq. (S3). The relation between T_{cs} and v_s is $T_{cs} = 2\Lambda e^{\gamma_E} \pi^{-1} \exp[-1/2N_0 |v_s|]$, where Λ is a cutoff for the high energy attraction and γ_E is Euler's constant. Similarly, for T_{ct} , we have $T_{ct} = 2\Lambda e^{\gamma_E} \pi^{-1} \exp[-1/2N_0 |v_t|]$. For the analysis, we use the transition temperatures rather than the interaction amplitudes as parameters.

In the basis $\{c_{\mathbf{k}\uparrow}^\dagger, c_{\mathbf{k}\downarrow}^\dagger, c_{-\mathbf{k}\uparrow}, c_{-\mathbf{k}\downarrow}\}$, the Hamiltonian (S1) for the clean case, that is $U_0(\mathbf{k} - \mathbf{k}') = 0$, may be written after mean field decoupling as a 4×4 matrix $[H]$,

$$[H] = \begin{bmatrix} \xi_{\mathbf{k}} + [\boldsymbol{\gamma}(\mathbf{k}) - \mathbf{B}] \cdot \boldsymbol{\sigma} & \Delta(\mathbf{k}) \\ \Delta^\dagger(\mathbf{k}) & -\xi_{\mathbf{k}} + [\boldsymbol{\gamma}(\mathbf{k}) + \mathbf{B}] \cdot \boldsymbol{\sigma} \end{bmatrix}. \quad (\text{S6})$$

The dispersion relation is determined by solving the equation

$$\det[E\hat{\sigma}_0 - [H]] = 0 \quad (\text{S7})$$

for E , where $\hat{\sigma}_0$ is the 4×4 unit matrix. We choose the phase of the singlet OP Δ_s to be 0. The coupling between the singlet and triplet order parameters imposes their relative phases such that $\mathbf{d}(\mathbf{k}) = i \text{sign}(E_Z) \hat{\gamma}(\mathbf{k}) \Delta_{tB} \hat{y}$ with Δ_{tB} real and positive. The physically relevant solution for the energy is

$$\begin{aligned} E(\xi_{\mathbf{k}}) &= \left(\xi_{\mathbf{k}}^2 + E_{SO}^2 + E_Z^2 + \Delta_s^2 + \Delta_{tB}^2 \right. \\ &\quad \left. - 2\sqrt{\xi_{\mathbf{k}}^2 (E_{SO}^2 + E_Z^2) + (|E_Z| \Delta_s - E_{SO} \Delta_{tB})^2} \right)^{1/2}. \end{aligned} \quad (\text{S8})$$

The dispersion $E(\xi_{\mathbf{k}})$ has a minimum at $\xi_{\mathbf{k}} = \sqrt{\rho^2 - P^2/\rho^2}$, where we introduced the notation $\rho = \sqrt{E_{\text{SO}}^2 + E_Z^2}$ and $P = |E_Z|\Delta_s - E_{\text{SO}}\Delta_{tB}$, which gives the superconducting energy gap

$$\Delta = \frac{1}{\rho} (E_{\text{SO}}\Delta_s + |E_Z|\Delta_{tB}). \quad (\text{S9})$$

B. Without inter-valley scattering: Quasiclassical Green functions

The coupled order parameters and density of states can be computed using quasiclassical Green functions. In the absence of inter-valley scattering, we obtain^{S1}

$$\nu(E) = 2N_0 \Re \left[\frac{\omega_n \text{sign}(\Sigma)}{\sqrt{2} [\Sigma - 2\rho^2 + \text{sign}(\Sigma)\sqrt{\Sigma^2 - 4P^2}]^{1/2}} \left(1 + \frac{|\Sigma|}{\sqrt{\Sigma^2 - 4P^2}} \right) \right]_{i\omega_n \rightarrow E+i\delta}, \quad (\text{S10})$$

$$\Delta_s = 2\pi T |v_s| \sum_{\omega_n > 0} \frac{1}{\sqrt{2} [\Sigma - 2\rho^2 + \sqrt{\Sigma^2 - 4P^2}]^{1/2}} \left[\Delta_s \left(1 + \frac{\Sigma - 2E_Z^2}{\sqrt{\Sigma^2 - 4P^2}} \right) + \Delta_{tB} \frac{2|E_Z|E_{\text{SO}}}{\sqrt{\Sigma^2 - 4P^2}} \right], \quad (\text{S11})$$

$$\Delta_{tB} = 2\pi T |v_t| \sum_{\omega_n > 0} \frac{1}{\sqrt{2} [\Sigma - 2\rho^2 + \sqrt{\Sigma^2 - 4P^2}]^{1/2}} \left[\Delta_{tB} \left(1 + \frac{\Sigma - 2E_{\text{SO}}^2}{\sqrt{\Sigma^2 - 4P^2}} \right) + \Delta_s \frac{2|E_Z|E_{\text{SO}}}{\sqrt{\Sigma^2 - 4P^2}} \right], \quad (\text{S12})$$

where $\omega_n = \pi T (2n + 1)$ are fermionic Matsubara frequencies and we introduced the notation $\Sigma = \omega_n^2 + \rho^2 + \Delta_s^2 + \Delta_{tB}^2$.

The density of states Eq. (S10) displays a superconducting energy gap Δ . Furthermore, there is a partial “mirage” gap^{S4} centered around $E = \pm \sqrt{\rho^2 + \Delta_s^2 + \Delta_{tB}^2}$.

In general, the coupled self-consistency equations can be solved numerically. The fit shown in the main text was obtained that way. However, simplifications are possible in the limit $E_{\text{SO}} \gg \Delta_0$, where Δ_0 is the zero-temperature, zero-field singlet order parameter. In that case, Eqs. (S11) and (S12) may be combined into one equation for the gap Δ ,

$$\frac{\left[2\pi T |v_s| \sum_{\omega_n > 0} \frac{1}{\sqrt{\omega_n^2 + \Delta^2}} - 1 \right] \left[2\pi T |v_t| \sum_{\omega_n > 0} \frac{1}{\sqrt{\omega_n^2 + \Delta^2}} - 1 \right]}{|v_t|E_{\text{SO}}^2 \left[2\pi T |v_s| \sum_{\omega_n > 0} \frac{1}{\sqrt{\omega_n^2 + \Delta^2}} - 1 \right] + |v_s|E_Z^2 \left[2\pi T |v_t| \sum_{\omega_n > 0} \frac{1}{\sqrt{\omega_n^2 + \Delta^2}} - 1 \right]} = 2\pi T \sum_{\omega_n > 0} \frac{1}{\sqrt{\omega_n^2 + \Delta^2}} \frac{1}{\omega_n^2 + \rho^2} \quad (\text{S13})$$

The density of states at $|E| \ll E_{\text{SO}}$ acquires a BCS form,

$$\nu(E) = \nu_0 \frac{|E|}{\sqrt{E^2 - \Delta^2}} \theta(|E| - \Delta). \quad (\text{S14})$$

C. With inter-valley scattering: Landau expansion

To study the effect of disorder, we resort to a perturbative treatment valid close to the critical temperature. Considering the model Hamiltonian above and using quasiclassical methods the difference of the thermodynamic potential in superconducting and normal state Ω may be written in the form of a Landau expansion as

$$(V^2 N_0)^{-1} \Omega(\Delta_s, \Delta_{tB}) = \Omega^{(2)} + \Omega^{(4)}. \quad (\text{S15})$$

Here $\Omega^{(2)}$ contains the terms quadratic in the OPs, and $\Omega^{(4)}$ contains the quartic terms. For $\Omega^{(2)}$, we have

$$\Omega^{(2)} = A_1 \Delta_s^2 + A_2 \Delta_{tB}^2 + 2A_3 \Delta_s \Delta_{tB}. \quad (\text{S16})$$

Denoting $\tilde{\omega}_n = \omega_n + \text{sgn}(\omega_n) \Gamma$, the coefficients are given as^{S5},

$$A_1 = 2\pi T \sum_{\omega_n > 0} \frac{\tilde{\omega}_n E_Z^2}{\omega_n [\tilde{\omega}_n (E_Z^2 + \omega_n^2) + \omega_n E_{\text{SO}}^2]} + \ln \frac{T}{T_{\text{cs}}}, \quad (\text{S17})$$

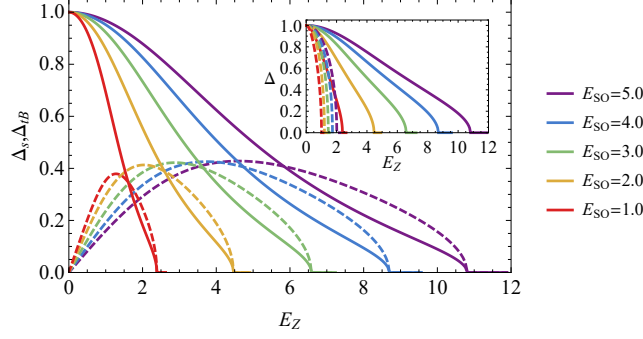


Figure S1 Effect of the magnitude of the spin-orbit coupling: The singlet Δ_s (solid lines) and triplet Δ_{tB} (dashed lines) OPs as a function of the field for different values of E_{SO} with parameters $T = 0.75T_{cs}$, $T_{ct} = 0.7T_{cs}$, $\Gamma = 0.001T_{cs}$. The inset shows the superconducting gap Δ for different values of E_{SO} and with the same parameters as the main graph, the solid lines are with the triplet component and the dashed lines are for a singlet-only superconductor ($T_{ct} = 0$). E_Z, E_{SO} are in units of T_{cs} . $\Delta, \Delta_s, \Delta_{tB}$ are normalized to the value of $\Delta = \Delta_s$ at $E_Z = 0$.

$$A_2 = 2\pi T \sum_{\omega_n > 0} \frac{\Gamma (E_Z^2 + \omega_n^2) + \omega_n E_{SO}^2}{\omega_n [\tilde{\omega}_n (E_Z^2 + \omega_n^2) + \omega_n E_{SO}^2]} + \ln \frac{T}{T_{ct}}, \quad (S18)$$

$$A_3 = 2\pi T \sum_{\omega_n > 0} \frac{(-E_Z)E_{SO}}{\tilde{\omega}_n (E_Z^2 + \omega_n^2) + \omega_n E_{SO}^2}. \quad (S19)$$

For succinctness, we do not provide here the full expression for $\Omega^{(4)}$ and only write the term corresponding to the singlet OP

$$\Omega_s^{(4)} = -\pi T_{cs} \sum_{\omega'_n > 0} D_1 (\omega'_n) \Delta_s^4, \quad (S20)$$

where

$$D_1 (\omega) = \frac{1}{2 [\tilde{\omega} (E_Z^2 + \omega^2) + \omega E_{SO}^2]^4} \left[-\omega (\omega \tilde{\omega} + E_{SO}^2)^4 + 2E_Z^2 \omega (\tilde{\omega}^2 - E_{SO}^2) (\omega \tilde{\omega} + E_{SO}^2)^2 + E_Z^4 (3\omega \tilde{\omega}^4 + 2E_{SO}^2 \tilde{\omega}^2 (\Gamma + \tilde{\omega}) - \omega E_{SO}^4) \right]. \quad (S21)$$

and where $\omega'_n = \pi T_{cs} (2n + 1)$. In the limit $E_{SO} = 0$ and no triplet OP, $\Delta_{tB} = 0$, derivation of the thermodynamic potential (S15) by the singlet OP reproduces the self consistency equation found in Ref.^{S6}. Equipped with the thermodynamic potential, the OPs are found by the process of minimization.

Using the Landau expansion, we can obtain a qualitative understanding of the way the different parameters affect Δ_s , Δ_{tB} and Δ as a function of the field. We start with the case of negligible inter-valley scattering. In Fig. S1, we see that for large enough E_{SO} the effect of increasing E_{SO} is only to stretch the lines for larger critical fields E_{Zc} but otherwise keeping the shape of lines as they are. In Fig. S2, we see that the effect of increasing T_{ct} is to obtain larger critical fields E_{Zc} by increasing the triplet component in the superconducting phase, specifically we see that for larger T_{ct} we get a steeper rise of the triplet component at low fields.

We now turn to the effect of disorder. The impurity scattering potential has a broadening effect on the peak of the density of states but does not affect the form of the effective order parameter Δ appearing in the density of states significantly (though the superconducting energy gap may differ), hence we use (S9) as an estimation also in the presence of weak inter-valley scattering. In the presence of the in-plane magnetic field, the scattering off the scalar impurities causes a spin flip with finite probability, and makes the scalar impurity to behave effectively as a magnetic impurity with a field-dependent concentration. While the problem is captured by the Abrikosov-Gorkov theory of magnetic impurities^{S7} in some parameter regimes, the general form of the self-consistency equation differs from the standard situation because the spin splitting E_{SO} intervenes as an additional energy scale.

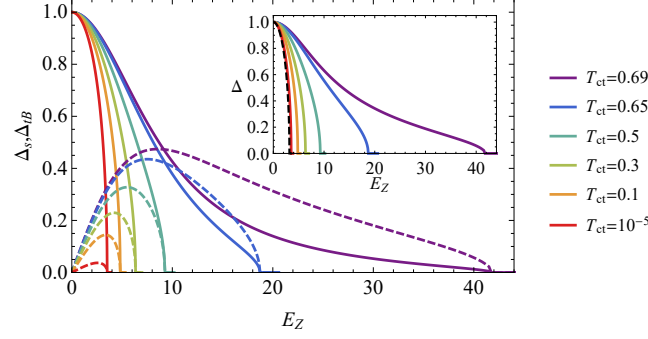


Figure S2 Effect of the triplet pairing: The singlet Δ_s (solid lines) and triplet Δ_{tB} (dashed lines) OPs as a function of the field for different values of T_{ct} with parameters $T = 0.7T_{cs}$, $E_{SO} = 8.0T_{cs}$, $\Gamma = 0$. The inset shows the superconducting gap Δ for different values of T_{ct} and with the same parameters as the main graph. The black dashed line is the superconducting gap for a singlet-only superconductor ($T_{ct} = 0$). E_Z, T_{ct} are in units of T_{cs} . $\Delta, \Delta_s, \Delta_{tB}$ are normalized to the value of $\Delta = \Delta_s$ at $E_Z = 0$.

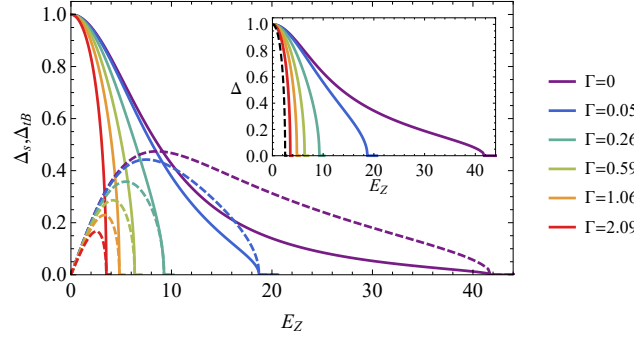


Figure S3 Effect of disorder: The singlet Δ_s (solid lines) and triplet Δ_{tB} (dashed lines) OPs as a function of the field for different values of Γ with parameters $T = 0.7T_{cs}$, $E_{SO} = 8.0T_{cs}$, $T_{ct} = 0.69T_{cs}$. The inset shows the superconducting gap Δ for different values of Γ and with the same parameters as the main graph. The red dashed line is the superconducting gap for a singlet-only superconductor ($T_{ct} = 0$), and with $\Gamma = 2.09T_{cs}$. E_Z, Γ are in units of T_{cs} . $\Delta, \Delta_s, \Delta_{tB}$ are normalized to the value of $\Delta = \Delta_s$ at $E_Z = 0$.

The parameters corresponding to the lines with the highest critical fields in Figs. S2 and S3 are identical. The Γ parameters in Fig. S3 were chosen so that identical colors in Figs. S2 and S3 will have approximately the same critical field. In Fig. S3 we see that by increasing Γ we negate the affect of having $T_{ct} > 0$. Comparison of the OPs suppression obtained in Fig. S2 by decreasing T_{ct} to the suppression obtained in Fig. S3 by increasing Γ shows that in the latter process we can retain a relatively steep increase of the triplet OP even for small critical fields, while in Fig. S2 the decrease in the critical field is accompanied by a faster decrease in slope of the triplet. The reason for this is that, even though increasing Γ in Fig. S3 suppresses superconductivity, we still keep a high T_{ct} , which strengthens the triplet component, while in Fig. S2 the suppression of superconductivity is achieved by direct suppression of the triplet component. The gap contains contributions of both the triplet and singlet order parameters. As the triplet order parameter is affected more strongly by a suppression of T_{ct} than by increase in Γ the same is true for the gap. Compared to the triplet order parameter taken separately, the distinction between $\Delta(H)$ in the two cases is less pronounced as long as the singlet order parameter makes a dominant contribution to the gap.

II. THE SAMPLE AND EXPERIMENTAL METHODS

The devices reported in this work were fabricated in a similar method to those reported in ref^{S8}. First, NbSe₂ was exfoliated within a glovebox with an inert N₂ environment onto a silicon chip covered with 285nm of SiO₂. Next, WSe₂ was exfoliated on a PDMS stamp and examined to look for thin flakes. Once a suitable flake was found, it was

aligned and brought into contact with a thin flake of NbSe₂. Next, the heterostructure was removed from the glovebox and tunnel contacts (5nm/80nm Ti/Au) were deposited on the WSe₂ barrier. Finally, ohmic contacts (5nm/80nm Ti/Au) were deposited directly on the NbSe₂ after Ar milling to remove oxide layers. The resulting device is shown in figure S4. The two junctions focused on in the main text are J7, on top of a 2ML NbSe₂ flake, with a tunneling resistance of $R_1 \approx 1.8\text{M}\Omega$, and J6, on top of a 4-8ML NbSe₂ region, with a resistance of $R_2 \approx 12\text{k}\Omega$.

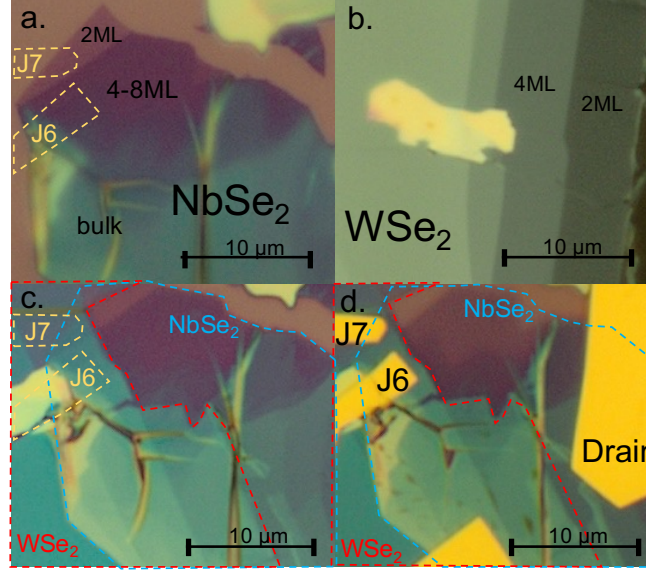


Figure S4 a. NbSe₂ exfoliated on SiO₂ from a PDMS stamp. Flake thickness is determined from the optical contrast. b. WSe₂ exfoliated on a PDMS stamp. Flake thickness is determined from the optical contrast. c. NbSe₂ – WSe₂ heterostructure formed by the deterministic transfer of the WSe₂. d. The final device with multiple tunnel junctions (J6,J7) and ohmic contacts (Drain).

As a part of the sample characterization the differential conductance of both junctions was measured at $T = 50\text{mK}$ (in a He³ – He⁴ dilution refrigerator) (shown in figure 2 of the main text). The extracted values for Δ are in line with the critical temperature T_c , estimated from the $G(V = 0)$ temperature dependence - see figure S5.

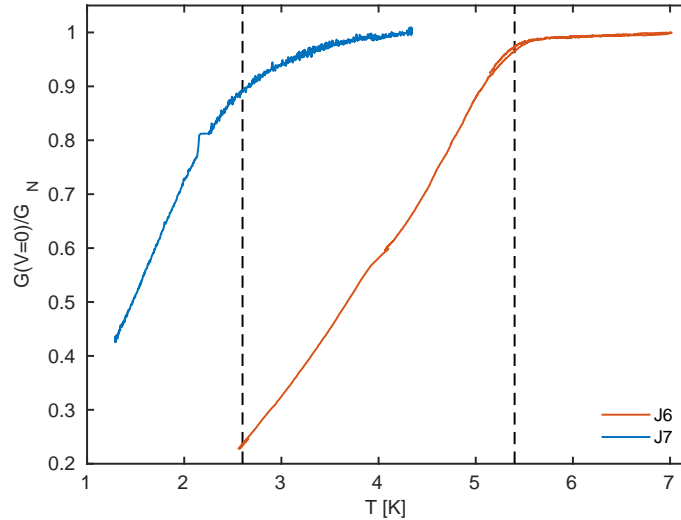


Figure S5 The temperature dependence of the zero voltage conductance, $G(V = 0)$, for devices J7 (2ML) and J6 (6ML).

The high field measurements were performed at the "Laboratoire National des Champs Magnétiques Intenses" in Grenoble, France. The magnet used allowed for magnetic fields up to $H = 36\text{T}$.

The sample was cooled down to $T = 1.25\text{K}$ in a pumped He^4 cryostat, and the differential conductance was measured using a standard lock-in technique with an excitation of $V_{\text{lock-in}} = 100\mu\text{V}$. Although the excitation voltage is relatively large, it does not lead to a significant smearing of the obtained spectrum as $eV_{\text{lock-in}} \ll 3.5k_B T \approx 360\mu\text{eV}$ (where $3.5k_B T$ is the FWHM width of the Fermi distribution transition). Likewise the electrical noise, generated by the magnet flux noise is also smaller than the temperature - see figure S6. The sample was mounted on a rotating stage, the axis of which was perpendicular to the magnetic field. A field of $H = 2\text{T}$ was applied and the sample was rotated, while measuring the height of the coherence peaks. By maximizing the peak height the magnetic field was aligned with the plane of the sample, with a maximum deviation of up to 1° .

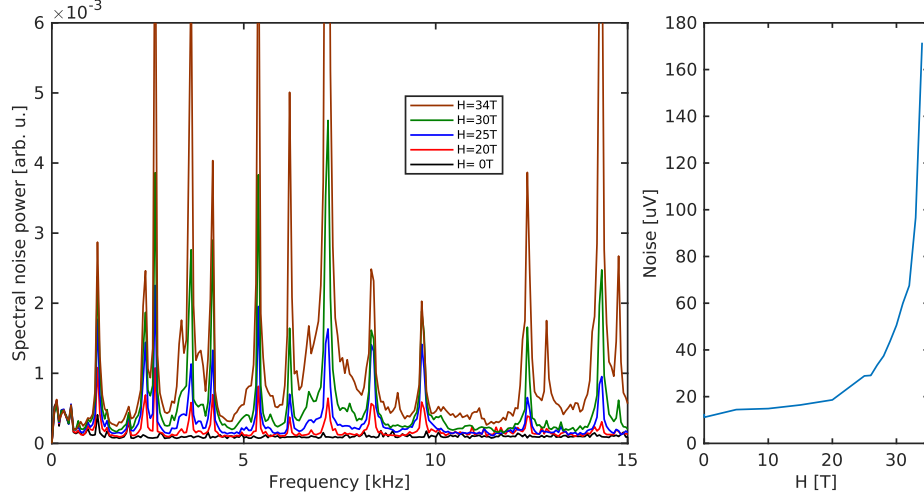


Figure S6 Electrical noise measured at $T = 1.2\text{K}$, across a $R = 10\text{k}\Omega$ resistor in a bandwidth of DC – 32kHz, as a function of the magnetic field. The left panel show the noise spectrum, while the right one shows the integrated noise voltage.

A. $G(V)$ curve fitting

With the main goal of determining the order parameter as a function of the magnetic field, $\Delta(H)$, the following heuristic approach was adopted. Without a proper microscopic theory to describe the soft gapped spectrum in presence of weak inter-valley scattering, and with limited ability to discern the details of the density of states (DOS) at $T = 1.3\text{K}$, the simplest approach to take is to try several different models for the $G(V)$ traces and compare the results. Even though there are countless models that one can utilize the discussion here is limited to the following three: an effective temperature T^* with a BCS DOS, an Abrikosov-Gorkov DOS (AG DOS)^{S9} and a Dynes DOS^{S10}. At finite temperatures the $G(V)$ curve is obtained by convolving the DOS with a distribution $\approx 3.5k_B T$ wide (FWHM): $G(V) = \frac{1}{eR} \int_{-\infty}^{\infty} dE N(E) \frac{\partial f(E-V)}{\partial V}$. If $\approx 3.5k_B T \approx \Delta$ this leads to a finite conductance at zero voltage bias (i.e. a soft gap). The Abrikosov-Gorkov depairing model lowers the spectral gap below the order parameter Δ . When the depairing energy equals the order parameter, $\alpha(H) = \Delta(H)$ this leads to a gapless state, but even when $\alpha(H) < \Delta(H)$ along with a finite temperature the resulting $G(V)$ trace can be gapless. Lastly, the Dynes DOS is non-zero at $E = 0$, directly leading to a soft gap. To illustrate this a simple example is shown in figure S7 - the top panel show the BCS, Abrikosov-Gorkov and Dynes densities of states, as well as the distribution function $\frac{\partial f(E-V)}{\partial V}$ for some parameter values, while the bottom panel shows the corresponding differential conductance traces. Although the BCS and the Abrikosov-Gorkov DOS' are fully gapped the resulting spectra are quite similar, and are in fact gapless.

The parameters for the effective temperature model were the (field dependent) order parameter $\Delta(H)$ and the temperature $T^*(H)$. For the Abrikosov-Gorkov and Dynes fits the temperature was fixed to $T = 1.25\text{K}$, while the depairing and Dynes energies were fitting parameters. The $\Delta(H)$ dependence obtained in this way, for both junctions and all three models, is shown on figure S8.

It is important to note that the values of these extra field dependent parameters, have no physical significance: the gap value is not self-consistently determined, nor should they be interpreted in the context of their usual meaning.

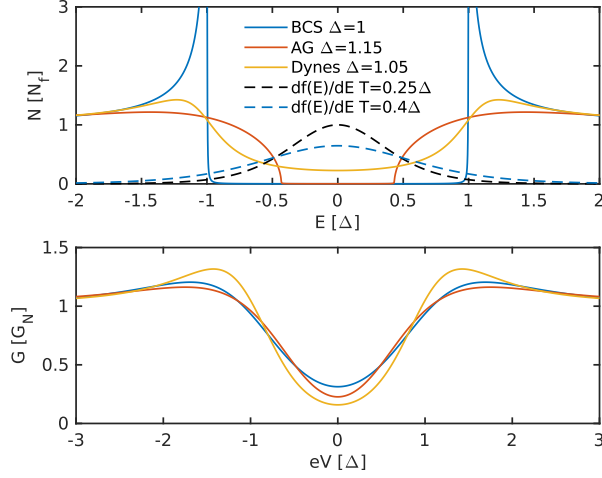


Figure S7 Top: The BCS density of states (blue, $\Delta = 1$), the Abrikosov-Gorkov one (red, $\Delta = 1.15$, $\alpha = 0.38$) and the Dynes one (yellow, $\Delta = 1.05$, $\Gamma = 0.24$). The dashed the (derivative of the) Fermi distribution function for $T = 0.25\Delta$ (black) and $T = 0.4\Delta$ (blue). Bottom: the corresponding $G(V)$ traces. The BCS DOS was convolved with the higher temperature distribution function, while the other two were convolved with the lower temperature one.

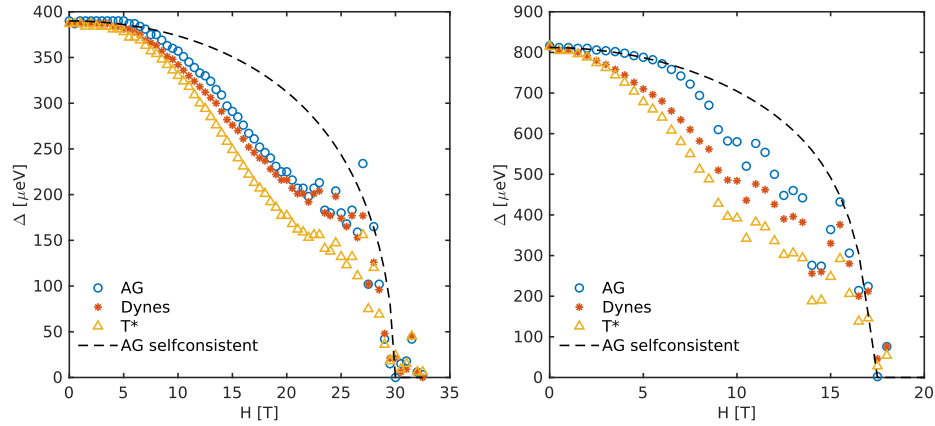


Figure S8 The extracted order parameters as function of the applied magnetic field using the three different $G(V)$ models, for the J7 (2ML, left panel), and J6 (4-8ML, right panel).

They are rather just phenomenological parameters used to describe the obtained $G(V)$ spectra. To illustrate this figure S9 shows the self-consistent and experimentally obtained Δ versus the Abrikosov-Gorkov and Dynes Γ parameters.

As this approach estimates Δ not based on the details of the $G(V)$ spectrum, but rather the energy scale of the (spectroscopic) gap, it is important to show that this is a robust feature. To this end figure S10 shows the $G(V)$ data from J7 at $H = 20\text{T}$, as well as several theoretical traces. The first of which is the Abrikosov-Gorkov fit, followed by two traces with the same gap, but different depairing values, which demonstrate that the energy scale of the gap is dominantly set by Δ while the depth of the gap at $V = 0$ is set by the depairing. The last trace shows that the gap is significantly different than the one found at $H = 0$, contrary to what one might naively infer based on the colorplots shown in figure 2 of the main text.

Additionally the error of the Δ estimation can be performed in the following way: the log-likelihood distribution for the fitting parameters (given the data) is given by

$$\tilde{p}(\Delta, \tilde{x}) = -\frac{\langle (G_i - f(V_i, \Delta, \tilde{x}))^2 \rangle_i}{2\sigma^2}$$

where \tilde{x} stands for the additional model-dependent parameters and $\langle \dots \rangle_i$ denotes the average over all of the acquired points. σ , the noise of the measurement, can be estimated either directly from data, or by the root-mean-square error

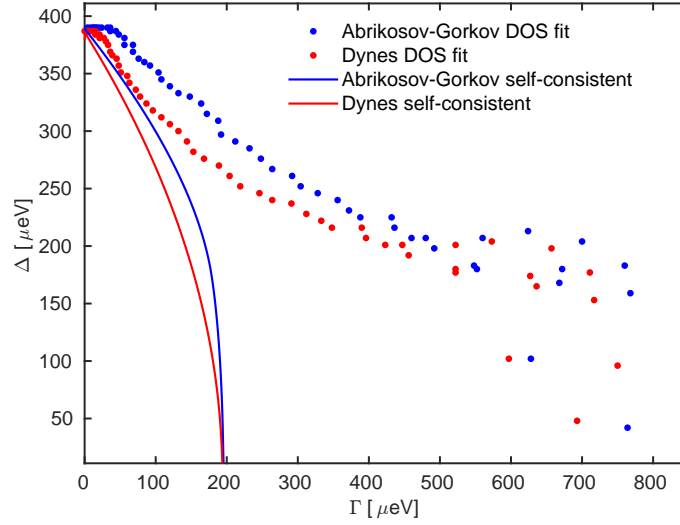


Figure S9 The order parameter Δ as a function of the Abrikosov-Gorkov depairing (blue) and the Dynes energy (red) for J7, obtained from the fitting (dots) and the self-consistent gap equation (full lines).

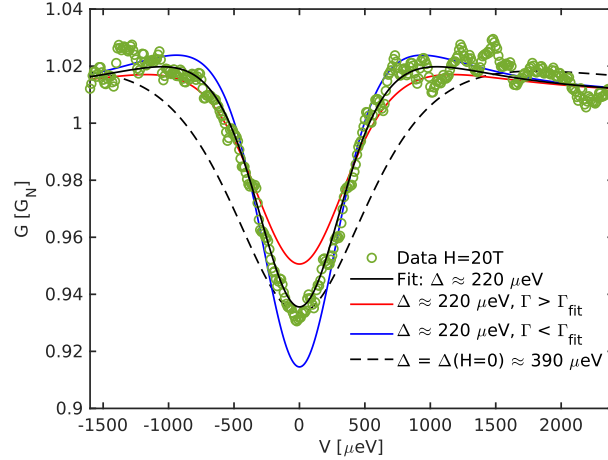


Figure S10 The experimental data from J7 at $H = 20\text{T}$ (green circles), the Abrikosov-Gorkov fit (solid black) and two traces with the same Δ but different depairings and a trace with $\Delta = \Delta(H = 0)$ with a depairing which fits the "depth" of the spectroscopic gap.

of the fit, both of which give similar results. The log-likelihood is not necessarily quadratic in Δ , as the fitting problem is nonlinear, but close to the maximum-likelihood point it can be approximately quadratic. Therefore by fitting \tilde{p} near its maximal point with $-\frac{(\Delta - \tilde{\Delta})^2}{2\delta_\Delta^2} + c$, where c is related to the RMSE and $\tilde{\Delta}$ is the best fit value, we obtain an estimate of the fit uncertainty δ_Δ . The Abrikosov-Gorkov $\Delta(H)$ curve with errors estimated in this way is shown in figure 3 of the main text. We find that the uncertainty of the extracted values of Δ is roughly equal to the spread of the data, regardless of the $G(V)$ model. The experimental $G(V)$ traces and the Abrikosov-Gorkov fits are shown on figure 2 of the main text. The fits obtained using the other two models are almost indistinguishable from the Abrikosov-Gorkov one.

References

- [S1] S. Ilic, J.S. Meyer, and M. Houzet, in preparation.
- [S2] Haim, M. and Möckli, D. and Khodas, M., Phys. Rev. B 102, 214513 (2020).

- [S3] Möckli, David and Khodas, Maxim, Phys. Rev. B 99, 180505 (2019).
- [S4] Belzig G. Tang, C. Bruder, and W. Belzig, preprint arXiv:2011.07080.
- [S5] Möckli, David and Khodas, Maxim, Rev. B 101, 014510 (2020)
- [S6] Maki, K. Physics Physique Fizika 1, 127 (1964)
- [S7] Abrikosov, A. A. and Gor'kov, L. P, JETP 12, 1243 (1961).
- [S8] Dvir, T. and Massee, F. and Attias, L. and Khodas, M. and Aprili, M. and Quay, C. H. L. and Steinberg, H., Nature Communications 9, 598 (2018)
- [S9] Skalski, S. and Betbeder-Matibet, O. and Weiss, P.R. Phys. Rev. 136, A1500 (1964)
- [S10] Dynes, R. C. and Narayanamurti, V. and Garno, J. P., Physical Review Letters 21, 509 (1978)

* These two authors contributed equally